Materials & Design
Volume 182, 2019, 108046
https://doi.org/10.1016/j.matdes.2019.108046

Evaluation via powder metallurgy of nano-reinforced iron powders developed for selective laser melting applications

Andre Mussatto [1, 2, 3, a], Robert Groarke [1, 2, 3], Ahmed A-Hameed [1, 3], Inam UI Ahad [1, 2, 3], Rajani K. Vijayaraghavan [2, 3, 4], Aidan O'Neill [5], Patrick McNally [2, 3, 4], Yan Delaure [1, 2, 3], Dermot Brabazon [1, 2, 3]

[1] School of Mechanical and Manufacturing Engineering, Dublin City University, Glasnevin, Ireland

[2] I-Form Advanced Manufacturing Research Centre, Dublin City University, Glasnevin, Ireland

[3] Advanced Processing Technology Research Centre, Dublin City University, Glasnevin, Ireland

[4] School of Electronic Engineering, Dublin City University, Glasnevin, Ireland

[5] Castolin Eutectic, Magna Business Park, 36 Magna Avenue, Citywest, Dublin 24, Ireland

[a] Corresponding author: andre.mussatto2@mail.dcu.ie

Highlights

- Powders were successfully developed via an optimised ball milling mixing technique.
- A uniform and consistent layer of nano SiC particles with a strong adherence onto the surface of the 316L particles was obtained.
- The developed nano SiC coated 316L powder presented superior flowability characteristics in comparison to the sieved 316L powder.
- The addition of nano SiC to 316L has significantly improved the hardness of sintered samples.
- Iron silicide and complex carbides precipitates resulted from the dissolution of SiC into the 316L matrix.

Abstract

In this work, a gas atomised stainless steel AISI 316L powder was used as metal matrix and SiC was employed as a nano reinforcement. The powders were experimentally characterised to determine the effect of the morphology, size, and levels of reinforcement on the powder flowability. The powder was developed via the powder metallurgy route and the effect of material, process conditions and various levels of reinforcement were investigated through the microhardness of the sintered samples. Sintered samples produced from the 316L+SiC+PVA powder mixes presented improved hardness. Analysis of the Energy Dispersive X-ray measurements detected high intensity levels of carbon and silicon on the surface of the reinforced 316L particles. In terms of measured powder rheology, the 6 wt. % SiC coated 316L provided the highest flowability of the prepared SiC coated 316L powders and a much higher flowability than the as received 316L powder. All prepared SiC coated 316L powders showed good flowability and highly repeatable powder rheology. The high degree of flowability was attributed to the particle spherical morphology, the narrow range of particle size distribution and also the coating of nano SiC particles on the 316L particles which were found to act in this case as a solid lubricant. A successful homogeneous and uniform reinforcement of SiC onto the surface particles was resultant from the established mixing technique. While the nano-SiC improved the powder fluidity, the obtained improvement in hardness was also due to the nano-SiC dissolution and resultant precipitates formed during the thermal treatment.

Materials & Design
Volume 182, 2019, 108046
https://doi.org/10.1016/j.matdes.2019.108046

Graphical Abstract

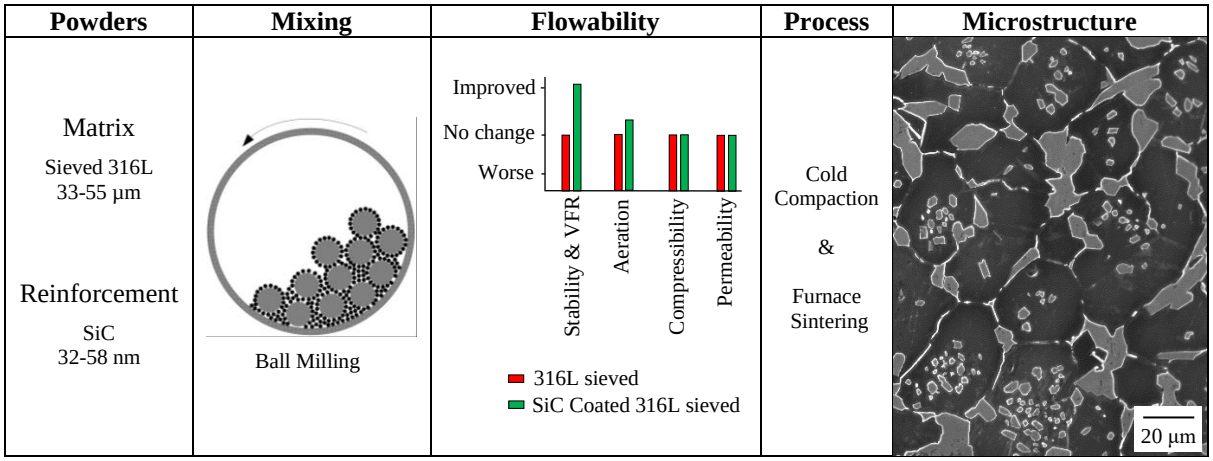

Keywords: Selective laser melting; Metal matrix composites; Nano reinforcement; Powder metallurgy; Stainless steel; Powder rheology

1. Introduction

In recent years, metal matrix composites (MMCs) reinforced with nano-particles reached a degree of maturity, with promising properties suitable for numerous structural and functional applications. These composites consist of one or more reinforcement materials, embedded into and featuring mechanical and physical properties very different from those of the metal matrix [1]. Nano-reinforcements can improve the base material in terms of mechanical strength and wear resistance, and retain composite properties at elevated temperatures [2]. Powder metallurgy (PM) routes are extensively used for new composite composition investigation. Besides being inexpensive and simple, the PM process is suitable for the synthesis of micro- and nano-ceramic reinforced MMCs, in addition to the resulting lower extent of material usage and waste generation [3–7].

The properties of the powders have a major impact on the packing ability and spreading performance of the consolidation method applied. In fact, it is well known that particle size, size distribution, shape and surface texture influence flowability and packability of powders, and that chemical composition, entrapped gas and oxidation influence their processability, energy input requirements and reactions [8–10]. The homogeneous mixing of reinforcement with matrix powders is a critical step to process MMCs, as it can have a significant influence on mechanical properties and production of defects [11,12]. Achieving a homogeneous distribution of the reinforcement in the matrix can be difficult. However, it has been reported that low energy milling enables fine reinforcement particles to adhere onto the surface of large matrix particles [13,14]. To date, several researchers attempted to obtain homogeneous blend of powders [15–20]. However, a processing route to obtain consistently good homogenous mixtures, still remains elusive, due for example to reinforcement particles clustering and reinforcement falling from the surface of matrix particles due to lack of adherence.

The rheological properties of metal powders are very important for both PM and selective laser melting (SLM) processes. In PM, a powder with poor flow characteristics may result in uneven compactions which can cause sample distortion, porosity and density anisotropy and stress concentrations [21,22]. Similarly, powder flow characteristics are key for the powder bed system to form uniform and consistent layers of powder [23,24]. Powder flow can be improved by particle surface smoothing, uniform particles size, reduced cohesion and increasing particle density and rounding. Powder flow can be influenced by particles with high friction, high mechanical interlocking, temperature, high moisture content, electrostatic charge, consolidation, process related variables and aeration of cohesive and non-cohesive powders [25]. It is recently further reported that fine powders, those below 30 µm, often exhibit poor flow and tendency to agglomeration as a result of higher Van der Waals forces [26]. The effect of particle size distribution studied by Ashcroft et al. showed that powders with narrower width of particle size distribution provided better flowability and produced parts with higher hardness and tensile strength [27]. Therefore , it was suggested that a better all-around combination of properties is obtained with an average particle size in the range of 30-45 µm [28].

A considerable amount of research has been performed in attempting to characterise the rheological behaviour of powders [29–34]. However, they concentrate on a single material type of powder, and to date there is no rheological records related to flow behaviour of nano-SiC reinforced steel powder mixtures. Therefore, this study was completed in order to have this information to better develop feedstock powders for processes like SLM and PM for the production of MMCs with improved properties. While most commercial metal matrix composites are aluminium based, steel based metal matrix composites are can be used in a variety of applications. For example, 316 reinforced by SiC can offer corrosion resistance with increased stiffness as may be required in marine, fuel processing or vehicle fuel line, aerospace or food processing applications. Other applications could include armour plating and vehicle mechanisms where higher stiffness and/or wear resistance are required compared to what can be achieved with aluminium matrix composites. It is worth noting that moving mechanical components with higher stiffness can provide an important efficiency of energy transfer and hence energy saving.

In this work, an iron based powder was used as metal matrix and nano SiC was added as reinforcement. In order to assess the potential for these powders to be used within the SLM and PM process, they were first experimentally characterised to determine the effect of the morphology, size, and nano reinforcement on the powder flowability. Then the powders were assessed via the PM route and the effect of various levels of reinforcement were investigated through the microhardness and microstructure of the sintered samples.

2. Experimental Work

2.1 Powders

In this study, a gas atomised micron size stainless steel AISI 316L powder supplied by Castolin Eutectic was used as metal matrix iron based material. Its chemical composition was 0.02 C, 1.47 Mn, 0.75 Si, 18.36 Cr, 12.20 Ni, 2.04 Mo, 0.04 P, 0.02 S, 0.10 N and Fe in balance (in wt.%). Nano size SiC powder (purity > 99 %) was obtained from US Research Nanomaterials Inc. and used as reinforcement. Polyvinyl alcohol (PVA) in powder form (> 99 % hydrolysed, Mw 98000) was obtained from Sigma-Aldrich and used as binding material.

Powder Sieving
The sieving was performed with an Endecotts Octagon 200CL sieve shaker and two woven wire mesh sieves of mesh sizes of 38 μm and 50 μm. Seven batches of 200 grams of the as received 316L powder were sieved. Each batch was sieved for 30 minutes in an amplitude of 3 mm.

Powder Quality Assessment
The particle size distribution of the 316L and PVA powders were obtained by laser diffraction measurements using a Malvern Mastersizer 3000. Both, the 316L and PVA particles were analysed in powder form. Additionally, the SiC powder was dispersed in de-ionised water and ultrasound was used to assist on the dispersion and break up of agglomerated particles. After two hours of sonication, the particle size of the SiC powder was measured by a Microtrac Nano-Flex 180° dynamic light scattering (DLS) system. Microstructural and morphological characterisation of the powders particles were conducted via scanning electron microscopy (SEM) using a Zeiss EVO LS-15 microscope.

2.2 Development of Powder

Powder Development process
The powder samples were prepared in terms of weight percent. The mixing of the powder samples was performed in a Pascal ball mill using a drum of 100 mm internal length and 90 mm internal diameter. Four 20 mm diameter spherical milling balls were used as mixing media and the rotation speed of the drum was set to 150 rpm.

Powder Flowability Analysis
Four batches of 100 grams of powder, each composed of sieved 316L + SiC 6 wt. % were prepared for mixing. The ball mill was set up as described previously and each batch of powders were mixed for four hours and then the four batches of powders were combined and mixed for another hour. For comparison, the flowability of the as received and sieved 316L powders were also investigated.

The stability, variable flow rate, aeration, compressibility and permeability characteristics of the three powders were investigated using a Freeman FT4 powder rheometer. The standard procedure of each test can be summarised to the following: The powders to be tested were placed inside cylindrical glass vessels of known volume. The stability test involved eight identical repeated tests with blade tip speed of 100 mm/s. Whereas for the variable

flow rate test the blade tip speed was gradually reduced in steps (100, 70, 40 to 10 mm/s) in the remaining four tests. In between each test a conditioning cycle was performed, where the blade passed through the powder eliminating any packing history. The various flow terms were then calculated from the work done in moving the blade through the powder from the top to the bottom of the vessel. The aeration test was conducted in a vessel mounted on a base with an air inlet port. During the test, the blade travelled downward helical path through the powder bulk. Between each of the different air flow rates (0, 2, 4, 6, 8 and 10 mm/s) the powder underwent a conditioning cycle. The incorporation of air into the powder was used to assess whether the powder flow properties change. The aeration measurements were then based on the reduction in flow energy. Prior the compressibility test, the powder samples were submitted to three conditioning cycles. Then, the blade was replaced by a vented piston which slowly consolidated the powder by applying a normal load in small increments between 1 to 15 kPa. The compressibility was then computed based on the percentage change in powder volume. The permeability test was run similarly to the compressibility test except by using a vessel base with an air inlet port. While the air velocity across the powder bed was maintained constant at 2 mm/s, the permeability of the powder was quantified by measuring the pressure drop across the powder bed whilst the applied normal pressure was gradually increased. The various flow terms and their definitions are given in Table 1.

Table 1 Flow terms and their definitions available for the FT4 Powder Rheometer.

Term	Definition
Basic Flowability Energy (BFE)	The energy needed to displace a conditioned powder sample during downwards testing.
Stability Index (SI)	The factor by which the measured flow energy changes during repeated testing or processing.
Flow Rate Index (FRI)	The factor by which the flow energy is changed when the flow rate (tip speed) is reduced by a factor of 10.
Specific Energy (SE)	The energy per gram needed to displace conditioned powder during upwards testing using a negative 5º helix (lifting to produce shear and no consolidation).
Conditioned Bulk Density (CBD)	Bulk density of a conditioned powder sample.
Aeration Ratio (AR_{10})	The factor by which the BFE is reduced when the sample is retested whilst being aerated at 10 mm/s of air velocity.
Aerated Energy (AE_{10})	The energy needed to displace an aerated powder sample whilst being aerated at 10 mm/s.
Compressibility (CPS_{15kPa} %)	Percentage by which the bulk density has increased with an applied normal stress of 15 kPa.
Pressure Drop (PD_{15kPa})	The decreased pressure while passing air through the powder at a speed of 2 mm/s while apply a normal stress of 15 kPa to powder.

Energy Dispersive X-ray Analysis

Energy Dispersive X-ray (EDX) analysis was mainly used to characterise the chemical composition present on the surface of the developed SiC coated 316L particles, but also to investigate if any trace of moisture, contamination and oxidation were present on them. The EDX analysis was performed on a sample of sieved 316L + SiC 6 wt. % powder, from the powder flowability analysis, using a SEM-EDX Hitachi S5500.

2.3 Fabrication of Composites

Composite Fabrication Process

The powder samples were prepared as mentioned previously in the powder development process. Sieved 316L was mixed with SiC (0, 1, 2, 3, 4, 5 and 6 wt. %) and 2 wt. % PVA, where each of the 15 grams of sample powder was mixed for four hours.

Powder compaction was performed using a Specac Atlas™ Autotouch 40T hydraulic press and a 20 mm in diameter pellet die. Before each compaction the die elements were lubricated with a thin layer of boron nitride powder. Three grams of powder was used per compaction which led to 1.5 mm thick and 20 mm diameter coin shaped green compacts. A compaction pressure of 500 MPa was held for three minutes and then slowly released.

The green compacts were placed onto alumina rectangular crucibles and then kept in a desiccator filled with silica gel until the next day when sintering was performed.

The sintering process was performed using a Lenton horizontal tube furnace, model LTF. The green compacts were sintered in argon atmosphere using a gas flow rate of one litre per minute. The green samples were heated up and cooled down at a rate of 5 °C per minute. When the temperature inside of the furnace reached 250 °C, 30 minutes temperature dwelling was applied. This allowed smooth initiation of thermal degradation of the PVA material within the samples. After this, the samples were heated up to 1200 °C and held at this temperature for three hours to enhance particle bonding and sample densification. Once the dwell time elapsed the temperature of the furnace was brought back down to room temperature at the rate previously mentioned.

Metallographic Sample Preparation
A Buehler Simplimet 2000 mounting press was used for the encapsulation of the samples in Bakelite. After this the samples were ground using SiC grinding papers of 240, 400, 800 and 1200 grit, and then pre-polished with Nylap cloths and 6 and 1 µm diamond suspensions, followed by a final polishing with a PSA polishing cloth and colloidal silica suspension of 50 nm, in a Grinder-Polisher Metken Forcipol 2V. The polished samples were etched with a solution composed of glycerol 20 %, nitric acid 20 % and hydrochloric acid 60 %.

Sintered samples Analysis
The hardness of the sintered samples was measured using a Leitz microhardness tester and the measurements were performed according to ASTM E92 standard, with 10 random indentations in each sample, indentations at the same direction as the load applied during compaction.

Microstructural analysis of the 316L (sieved) + SiC 6 wt. % composite was carried out using a triple-axis Jordan Valley Bede D1 high resolution X-ray diffraction (XRD) system with a copper (λ=1.5405 Å) radiation source operated at 45 kV and 40 mA, and on a Zeiss SUPRA 40 field emission scanning electron microscope (FESEM) equipped with a Broker Electron backscatter diffraction (EBSD) detector.

3. Results and Discussion

3.1 Powder Characterisation

As received powders
Ideally, for selective laser melting, powders with a Gaussian type of distribution is preferable. A powder with this type of distribution generally have good symmetric agreement about the mean particle diameter, D_{50}. This is normally the case for powders with narrow size distributions.

The as received 316L powder used in this study presented a negative skewed distribution which means that the powder contained a proportion of fine particles. These fine particles are better observable in the micrograph, see Figure 1 (a). From this type of particle size distribution, one would expect that this powder could provide a dense packing of the spread powder layer. However, a powder with a narrower width of particle size should provide a better powder flowability and enable production of parts with improved mechanical properties. Additionally, it can be seen from the micrograph that most of the particles had good sphericity. However, a small amount of the particles contained satellites. These sort of irregularity with the particles are not desired as they affect the flowability and packing ability of the powder.

The result of the particle size distribution analysis performed on the PVA powder showed that this powder contained a portion of particles from 10 to 50 µm. However, this powder contained a wide distribution, including some very large particles, see Figure 1 (b). The micrograph of the PVA powder showed that the particles were reasonably spherical and composed of several globular structures. These globular structures are common in these polymeric powders, as during the formation of the particles, macromolecules (long chain molecules) coil into globules.

Figure 1 (c) shows the particle size distribution of the SiC spherical powder. The plot indicates that the powder had a narrow distribution and a median particle size of 41 nm. It can be seen from the micrograph that the SiC particles tend to cluster, which is probably due to cohesive and electrostatic forces between the particles. The high degree of clustering of SiC particles may impose some difficulties on obtaining a homogeneous distribution of this material in the matrix powder. Local inhomogeneity and clustering of reinforcement particles influences the mechanical properties of the MMC, as clustered regions promote interface debonding and crack initiation and

have a negative effect on toughness and fatigue and tensile strength of the composite. To overcome this problem and to obtain a uniform dispersion of reinforcement in the MMC, a good mixing technique is required.

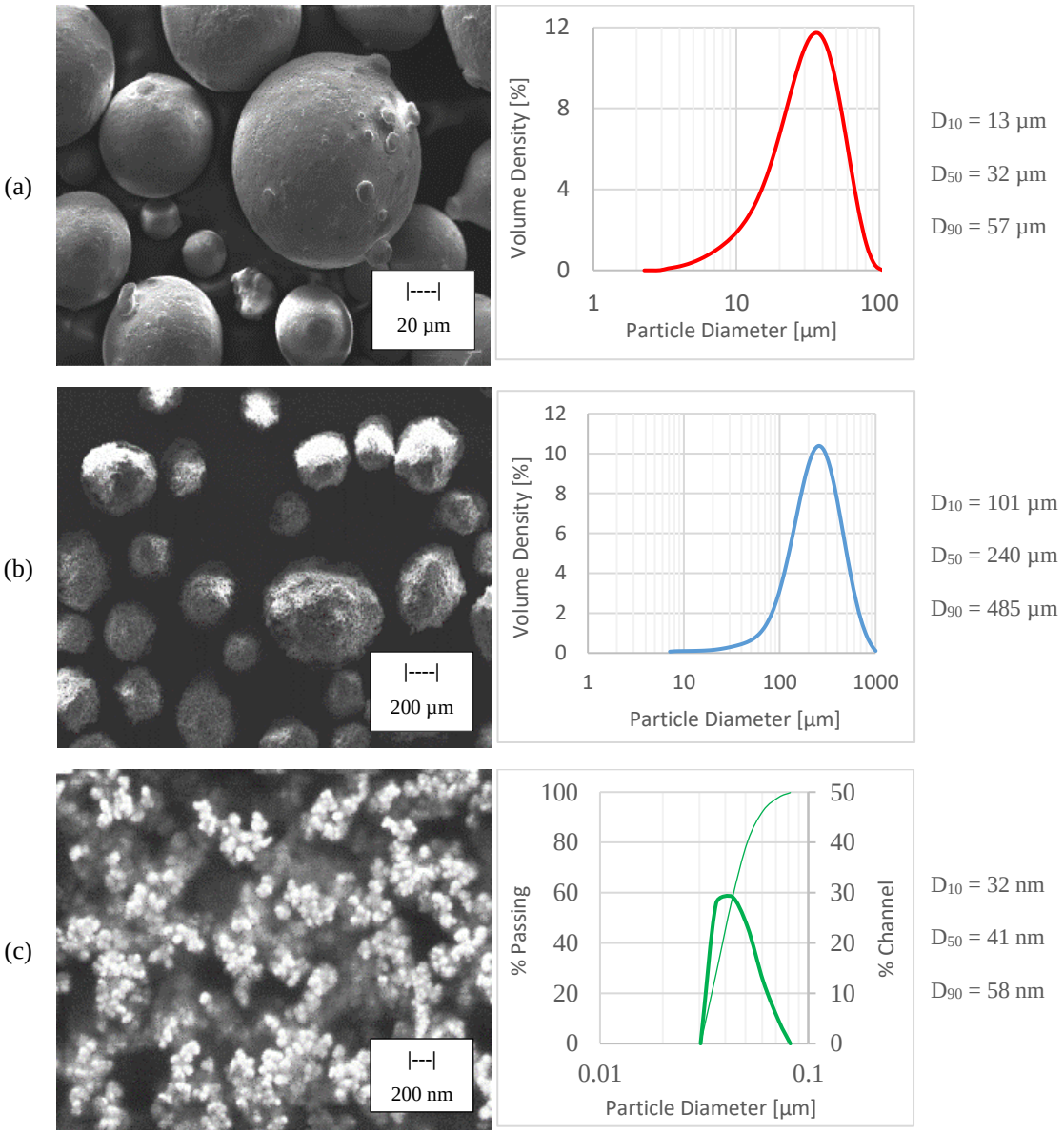

Figure 1 SEM micrographs and particle size distribution of the as received powders; (a) 316L, (b) PVA and (c) SiC.

Sieved 316L Powder

Sieving of the 316L powder was conducted in order to obtain a narrow particle size distribution and to remove very small particles and large irregular shaped particles. Particles smaller than 30 µm tend to agglomerate easily, present high level of cohesiveness and strongly vary packing fractions, thus affecting powder layer quality. Larger particles require a higher energy density for processing, affect the packing densification and thermal conductivity and could contribute to larger void sizes in printed parts reducing mechanical strength [35]. Therefore, sieving has the potential of improving powder flowability, which is very important for a powder bed system to form uniform and consistent layers of powder. Sieving to a discrete size range can also lead to a more consistent produced part porosity size in manufactured parts, thus facilitating their control and reduction through the optimisation of the processing parameters.

The resultant powder mass obtained from the sieved powder within 38 µm and 50 µm was approximately 40 % of the as received powder mass. The collected sieved powder was analysed in terms of particle size distribution and compared with the as received powder, Figure 2. When analysing the particle size distribution given by the

sieved powder it is seen that the D_{90} is slightly above 50 µm and that D_{10} is slightly below 38 µm. This is expected as some large irregular and elongated particles may have passed through the 50 µm mesh. On the other hand, particles that are smaller than 38 µm rarely remain in the 38 µm mesh. But in this case, some particles sized slightly smaller than the sieve mesh remained in the sieve. This could be due to the shape of these particles and due to too short sieving time. However, it can be said for this powder characteristics that the sieving time was performed near optimum conditions as equally - 5 µm for the small sieve mesh and + 5 µm for the large sieve mesh deviated from the expected particle size distribution. A longer sieving time would possibly allow more irregular shaped particles to pass through the 50 µm mesh and this would later impact on the powder bed quality. It is seen from the plot that volume density of the sieved powder increased, this was simply because the volume occupied by particles that were of the size D_{50} or close to the size D_{50} increased in comparison to the size D_{50} given by the as received powder. Additionally, it can also be said that powder size control with sieving is maximised as particles sphericity increases and topographic roughness smooths.

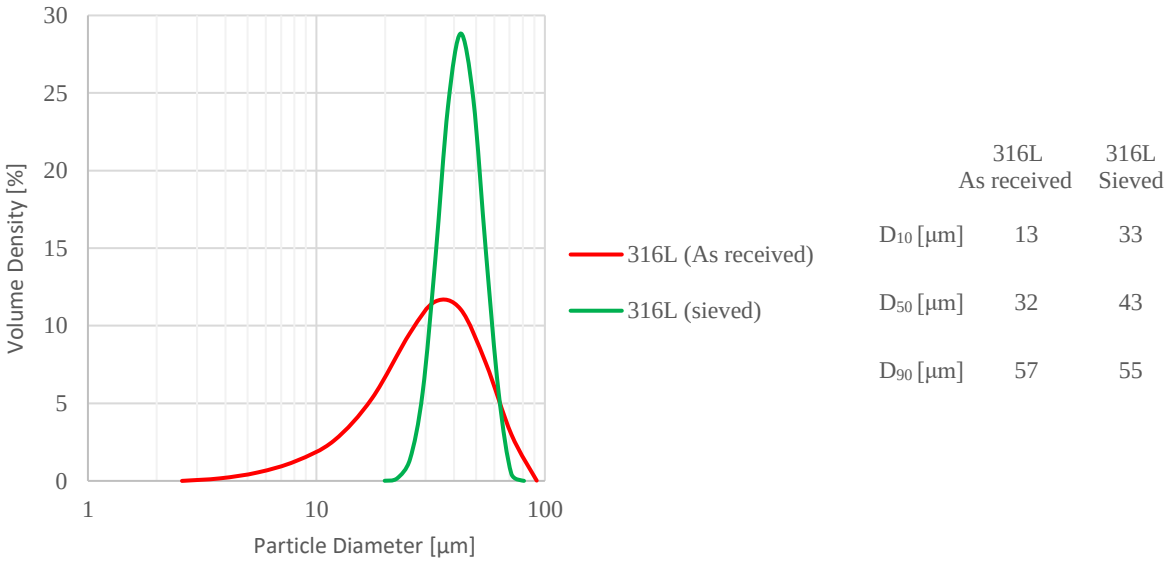

Figure 2 Particle size distribution of the sieved 316L powder.

3.2 Developed Powder Characterisation

Powder Flowability Assessment

The measured stability, variable flow rate, aeration, compressibility and permeability properties of the 316L as received, 316L sieved and 316L sieved + SiC 6 wt. % powders are shown in Figure 3 and Table 2.

The relative low basic flowability energy (BFE) measured from the three powders are characteristics found in powders with good flow properties, and this is due to many physical properties of the particles such as size, shape and surface texture. The specific energy (SE) measured from the powders indicated that they had low cohesion. A powder with low BFE and low SE is easy to displace due to the ease with which the particles move over each other, and this powder is more likely to have low conditioned bulk density (CBD). The CBD of the as received 316L powder is slightly higher than the other two powders because of its morphology and particle size and distribution. The stability index (SI) indicated that the powders were robust materials of good flow stability, and the flow rate index (FRI) suggested that the reinforced powder was much less sensitive to flow rate, such that it could be considered a flow rate insensitive powder. The superior reproducibility of the developed powder (316L sieved + SiC 6 wt. %) in comparison to the other tested powders is indicated by the calculated margin of error presented margin of error in Table 2. In addition, the change in the variable flow rate measured for this powder is lower than that recorded for the other powders. This indicates that this powder would be less sensitive to variations in process speed across various SLM or PM processing systems. In brief, the stability and variable flow rate results of the powders showed that the developed powder provided higher levels of repeatability and a very stable rheology.

The aeration results show that the powders were very sensitive to even very low air velocities, presenting a rapid rate of total energy reduction. With slightly increase in air velocity it is noted that the fluidisation state of the powders occurred, as the flow energies reduced to nearly zero. The higher value of the aeration energy (AE_{10})

measured from the as received 316L powder may be attributed to agglomeration and adhesion among its small sized particles. All the tested powders presented very high aeration ratios (AR_{10}) strongly suggesting that the powders were very sensitive to aeration and prone to fluidization, where this was even more pronounced with the sieved and reinforced 316L powders.

The compressibility test does not provide a direct measure of the flowability. However, it was used in this work to understand the behaviours of the powders such as during the roller or blade spreading of powder in SLM systems. The compressibility results indicate that the powders had moderate sensitivity to compression. However, the powders without the reinforcement had less change in volume even at high normal stresses. The slightly higher compressibility of the reinforced powder is explained by its nano coating of SiC which acted as a lubricant and thus impelling this powder to a higher compressibility. This is also visualised in the compressibility plot for this powder, as a sharp increase in compressibility. In such a case, like of the reinforced powder, compressibility may not be a good and true indicator for powder cohesiveness.

The permeability results show that compression has minimal or no effect on the permeability of the powders. The reinforced powder generated higher pressure drop across the powder bed than the other two powders, indicating either very small or limited number of channel between the particles. At this stage it is not known if the permeability level found in each of the powders influence the SLM process. A certain level of permeability is desirable to move a powder from one position to another, this allows gas to replace space vacated by the particles more easily. This case is analogous to the powder spreading process. A permeable powder has the capacity of retaining unwanted gas and release it during its processing. Such a powder then can have a detrimental effect on the SLM process and on the quality of its printed products.

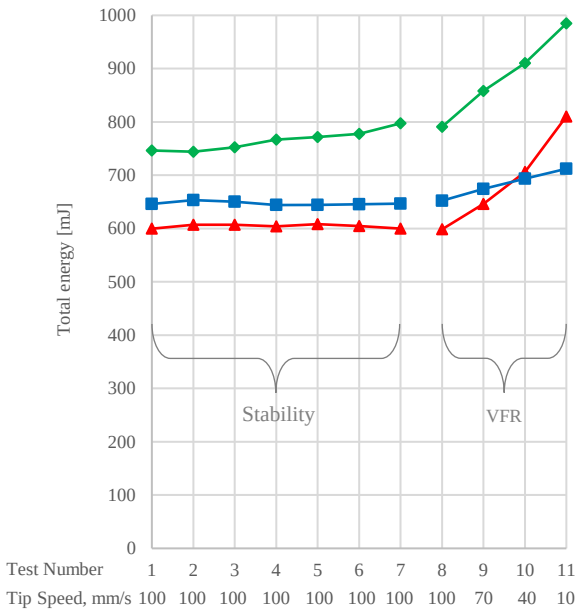

Stability and Variable Flow Rate

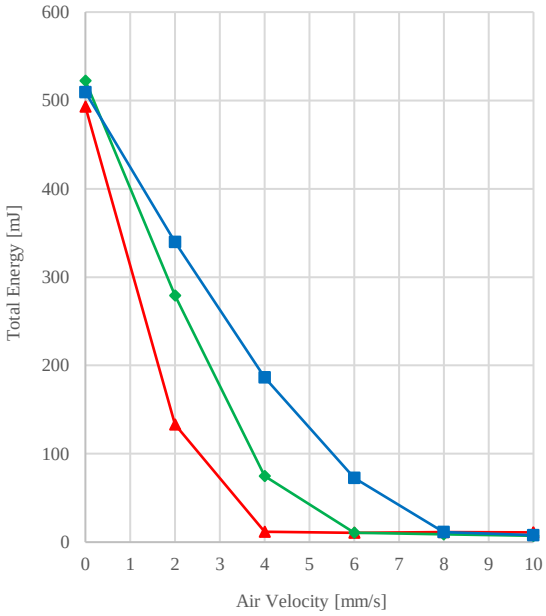

Aeration

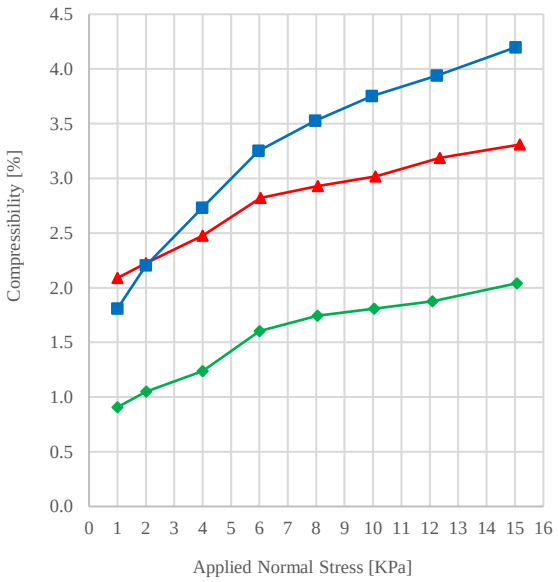

Compressibility

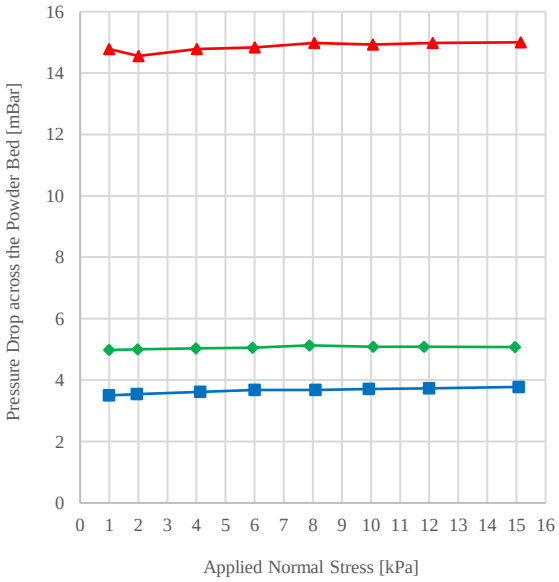

Permeability

316L (as received) 316L (sieved) 316L (sieved) + SiC 6 wt. %

Figure 3 Dynamic flow properties (stability, variable flow rate and aeration) and bulk properties (compressibility and permeability) of the powders (316L as received, 316L sieved and 316L sieved + SiC 6 wt.

%).

Table 2 Flowability characteristics of the powder samples.

Stability and Variable Flow Rate, n=3					
Series Name	BFE [mJ]	SI	FRI	SE [mJ/g]	CBD [g/ml]
316L (as received)	599.90	1.00	1.35	1.74	5.15
Margin of error (95% C.I.)	118.51	0.05	0.03	0.27	0.04
316L (sieved)	797.39	1.07	1.25	1.88	4.85
Margin of error (95% C.I.)	142.28	0.11	0.09	0.21	0.05
316L (sieved) + SiC 6 wt. %	646.80	1.00	1.09	2.96	3.46
Margin of error (95% C.I.)	32.75	0.08	0.04	0.14	0.16
Aeration, n=1					
Series Name	BFE [mJ]		AE_10 [mJ]		AR_10
316L (as received)	493.00		10.84		45.46
316L (sieved)	522.21		7.20		72.58
316L (sieved) + SiC 6 wt. %	509.35		7.89		64.53
Compressibility, n=1					
Series Name	CBD [g/ml]		CPS_{15kPa} [%]		
316L (as received)	5.21		3.31		
316L (sieved)	4.85		2.04		
316L (sieved) + SiC 6 wt. %	3.48		4.20		
Permeability, n=1					
Series Name	CBD [g/ml]		PD_{15kPa} [mBar]		
316L (as received)	5.35		15.00		
316L (sieved)	5.08		5.08		
316L (sieved) + SiC 6 wt. %	3.65		3.78		

Powder Topography and Chemical Analysis

Figure 4 (a) and (b) compares the topography of a 316L particle with a 6 wt. % SiC coated 316L particle. The porous coat of SiC onto the particle seen in Figure 4 (b), which is better seen in (c), was estimated to be 470 nm. Monte Carlo simulation (CASINO V2.51) was used to find the EDX settings for an ideal depth of interaction volume for the particle shown in Figure 4 (b). Figure 4 (d) illustrates the simulated scattering paths of electrons from the particle shown in Figure 4 (b). The path represented by the red colour are backscattered electrons and the path represented by the blue colour are secondary electrons (absorbed electrons). Based on the simulation, it is seen that majority of the chemical information was extracted from the SiC layer. However, energetic electrons could have penetrated the SiC layer and backscattered electrons having chemical information about the 316L. Figure 4 (e) shows the chemical composition measured from the surface of particle show in Figure 4 (b). As expected, very high concentrations of Silicon and Carbon were observed. Additionally, Iron, Nickel, Chromium, Manganese and Molybdenum were identified, indicating the main elements composing the 316L. The presence of these elements can be explained along with the presence of Silicon and Carbon. A significant amount of the Silicon and Carbon were from the applied coat, and the other elements were most likely satellites detached from the 316L particles crushed during the powder mixing process that adhered to the surface of 316L particles together with the SiC particles. It was found that 6.45 wt. % of Oxygen was present on the SiC 316L surface. Oxygen could negatively affect the SLM process and the printed product quality. Figure 4 (e) presents the surface chemical composition. It should be noted that EDX is not able to accurately quantify absolute elemental concentration for carbon and oxygen due to their low atomic weight but can be used to indicate relative difference between sample for these elements.

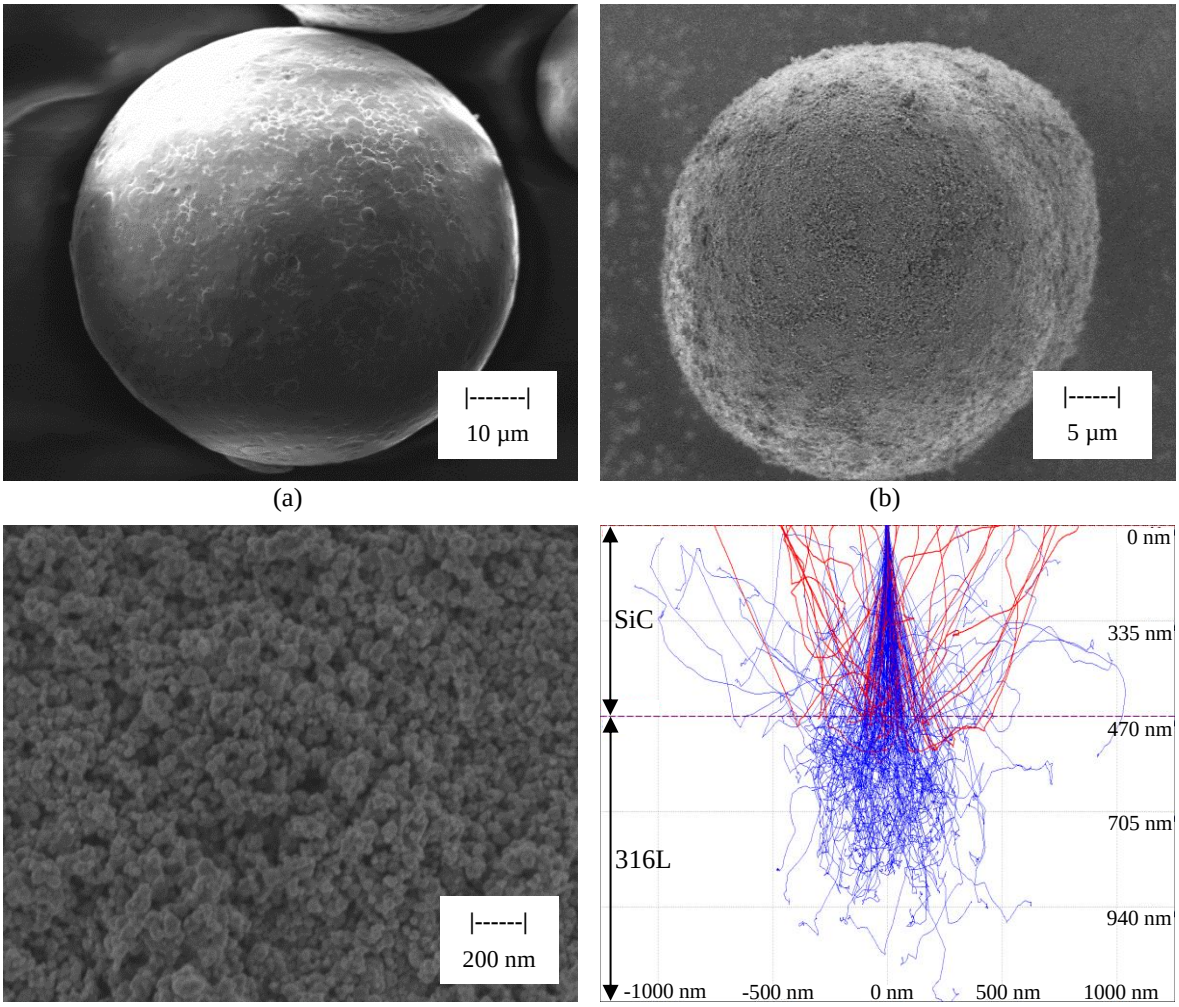

C	Si	Fe	Cr	O	Ni	Mn	Mo	Al
40.89 %	12.44 %	27.30 %	7.40 %	6.45 %	3.42 %	0.88 %	0.86 %	0.36 %

(e)

Figure 4 SEM micrographs comparing the topography of a 316L particle with a 6 wt. % SiC coated 316L particle, and the elemental composition obtained from the surface of the SiC coated 316L particle. (a) 316L particle, (b) 6 wt. % SiC coated 316L particle, (c) close-up view of the SiC nanoparticles coating the 316L particle, (d) Monte Carlo simulation displaying electron trajectories from the surface of the SiC coated 316L particle during the EDX analysis and (e) the measured chemical composition in terms of weight percent.

3.3 Sintered Samples Evaluation

Composite Microhardness

The Vickers hardness measure from the sintered samples is shown in Figure 5. Clearly, the addition of SiC to stainless steel 316L has improved the hardness remarkably. It is seen a nearly exponential relationship between the amount of reinforcement and hardness. The hardness results obtained in this experiment showed that small amount of SiC can significantly improve the hardness of stainless steel 316L. It is expected that this is importantly due to carbide segregation at grain boundary which restricts grain growth, hence further contributing towards enhancement of the hardness. Further hardness increase could potentially be achieved through further detailed investigation of the processing parameters. In general, these measurements give a good indication of what hardness to expect from the developed powders when processed via SLM.

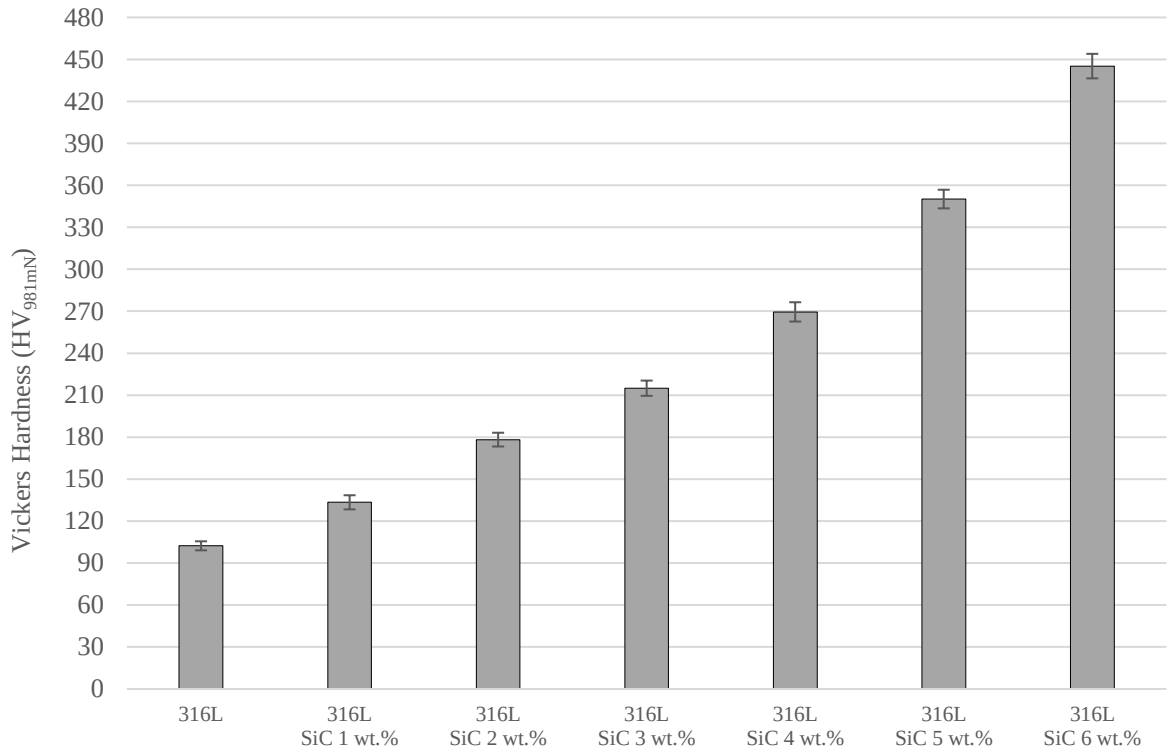

Figure 5 Vickers hardness results obtained from the sintered samples, n=3.

Composite Microstructure

The microstructures of the 316L samples prepared with different amounts of nano-SiC are shown in Figure 6 (a-g). The effect of adding SiC into the 316L matrix is clear on the presented micrographs. According to these micrographs, secondary phases were introduced by precipitation reactions involving the reinforcement and matrix elements. The numerous particle boundaries and angular pores seen in Figure 6 (a) are indicative of undersintering. Those particles lacking on contact points prevented the diffusion mechanism which is responsible for particle bonding, hence leading to porosity. On the other hand, a well sintered microstructure with low level of porosity and small rounded pores is seen in Figure 6 (g). The relative density $\rho_{relative}$ of the samples was determined by $\rho_{relative} = \rho_{measured} / \rho_{theoretical}$ using the method mentioned in our previous work [36]. The relationship between relative density and weight percent of SiC is presented in Figure 6 (h). It is seen that the relative density increases almost linearly with increasing of SiC content. Therefore, confirming the influence of nano SiC on sample densification. Differently, it was reported that the addition of reinforcement reduces the density of composites due to low reaction between the carbide and stainless steel particles [37,38] which was not found to be the case in this study.

The relative density of sintered samples is influenced by the volume of the porosities in the green samples. In this study, the volume of the porosities was reduced by the SiC nanoparticles filling effect during the compaction. Potentially, the SiC nanoparticles also assisted on forming contact points between the matrix particles. Therefore, maximising particle bonding and porosity reduction. The oxide layer on the surface of 316L particles has the capacity of inhibiting formation of sintering bridges, whereas internal oxides are known to be particularly detrimental to the microstructure as they may result in unwanted reactions. Elements such as carbon and silicon have been widely used for reduction of oxides. In principle, these reducing agents diffuse into the particles to form a new phase, either a solid or a gas. It was reported the silicon has the potential of impairing the oxidation in the early stage of sintering (low temperatures) and that carbon is more efficient at higher temperatures [39–41]. Therefore, as both of these elements were present in the reinforcing material, this could also be a factor behind the composite densification. It is well known that nano-scale particles exhibit a melting temperature which depends on the particle size [42–46]. This is because atoms near the surface have fewer bonds and neighbouring atoms, hence less energy is needed for them to leave the surface [47,48]. Here, the melting point depression of the SiC particles was calculated using the classical Gibbs-Thomson equation [49]. The theoretical relationship between melting temperature and particle size of SiC nanoparticles is shown in Figure 6 (i). It indicates that at the

sintering temperature (1200°C), nanoparticles as large as 12 nm melt. Therefore, suggesting that the SiC addition could have the lowered the melting point of the powder mixtures. Moreover, it could have acted as a fluxing agent facilitating particle diffusion. Hence, reducing microstructural porosity and enhancing composite densification.

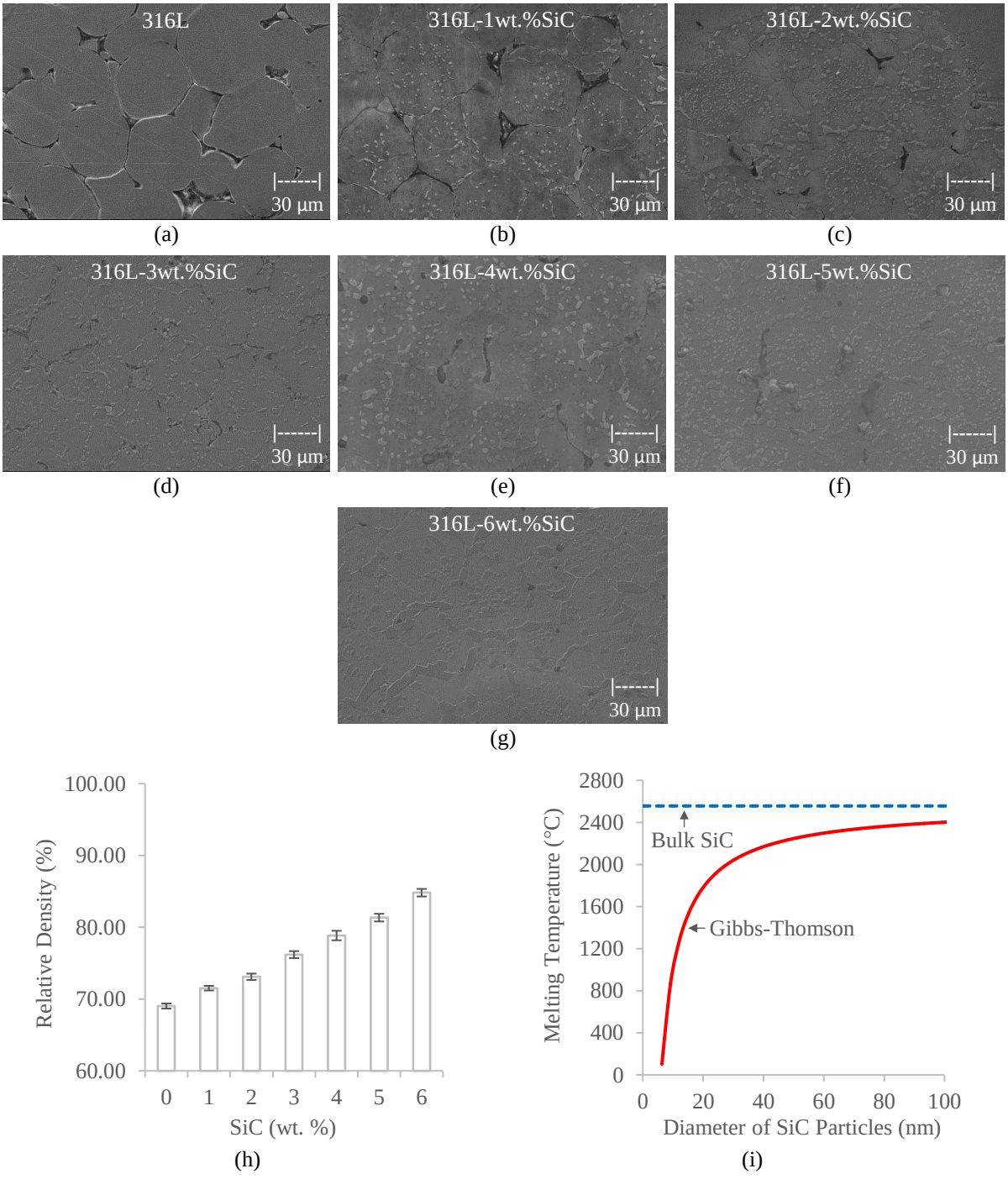

Figure 6 Scanning electron micrographs of the sintered composites (a-g), the composites relative density as a function of reinforcement percentage (h) and the theoretical relationship between melting temperature and particle size of Silicon Carbide nanoparticles (i).

Figure 7 shows x-ray diffractograms comparing the 316L and 316L-6wt.%SiC sintered samples. As seen in the diffractogram of the 316L sample, the effect of slow cooling induced the precipitation of Fe_2Si at the austenite grain boundary. The presence of austenite, iron silicide and chromium carbides phases were identified in the composite sample. However, SiC phases were absent in the composite. It is known that SiC undergoes significant change in thermal character at about 1200 °C and that it can decompose at this temperature when in contact with

iron [50–52]. This is the case here, where the decomposition of SiC led to the formation of silicon and carbon atoms at high temperatures. During the solidification, the silicon and carbon atoms dissolved into the austenite, leading to precipitations of the silicon rich phase Fe_2Si and the complex carbides Cr_3C_2 and Cr_7C_3. Fe_2Si is a ferromagnetic brittle phase of reduced corrosion resistance [53]. In general, chromium carbides have high abrasive resistance, but Cr_3C_2 has the highest oxidation and corrosion resistance and hardness of all [54,55]. However, chromium carbide precipitations are normally undesired since its presence is associated with decreased ductility and toughness. Nevertheless, they exhibit good resistance against shear deformation [56]. The increase in hardness in the analysed composite is attributed to the formed precipitates and grain refinement.

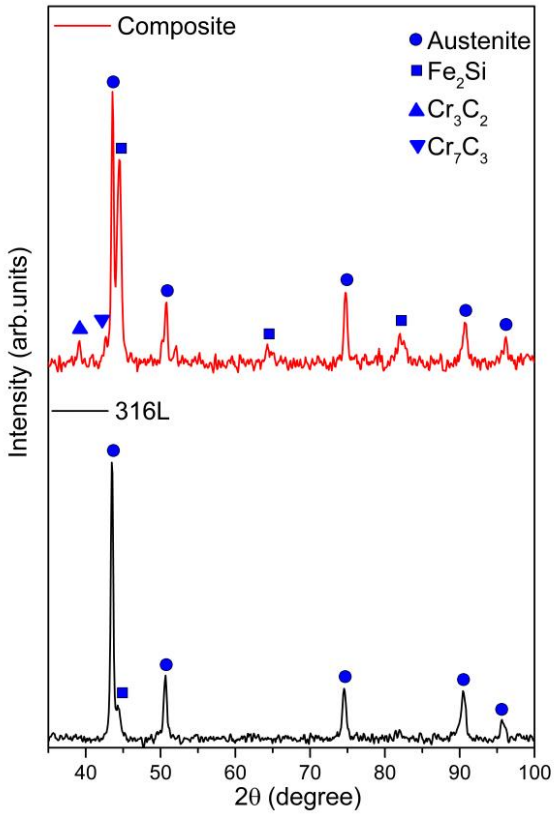

Figure 7 XRD diffractogram comparing the sintered 316L and 316L-6wt.%SiC composite.

The microstructural crystallographic characteristics of the 316L-6wt.%SiC composite was investigated via EBSD analysis. Figure 8 (a) shows the inverse pole figure map for the normal direction and (b) its respective index maps. There is no clear evolution of the austenite texture. On the other hand, the iron silicide phase revealed a preferential grain growth to the (001) and (120) crystallographic alignment. With the preferred grain growth being along the (001) direction distinctly. Conversely, the chromium carbides presented a relative weak (001) texture. Essentially, the (001) texture reflects vertical oriented grains, and this could be related to the solidification direction, as the top surface of the sample was under continuous argon flow and the bottom was in contact with the crucible. Therefore, the directional of growth occurred due to the indiced sintering high temperature gradient and low solidification rate. The phase analysis revealed the presence of austenite, iron silicide and chromium carbides, see Figure 8 (c). Thus, agreeing with the XRD data. Austenite phase of average size of 18.3 μm exhibited a fine surrounding boundary of iron silicide (average grain size 1.6 μm) surrounded in turn by chromium carbides (average size 5.8 μm). These precipitates were also present dispersed in the centre of austenite phase. These resulted as due to the slow cooling iron silicide and chromium carbides nucleated and formed at the austenite grain boundaries and in the interior of the austenite grains. However, the precipitates formed in the interior of the austenite grains were oriented short-needle-like crystals. The formation of precipitates around the austenite grain boundaries prevented grain growth. Thus, resulting in fine austenite grains. Figure 8 (d) shows the morphology of the precipitated irregular columnar grains. The presence of strain in the crystal lattice is supported by the changes observed in the EBSD kikuchi diffraction patterns and by the shift in the XRD peaks observed from the composite and matrix diffractogram comparison. In this composite, the strain could have been induced as a result of the precipitations and mismatch in the coefficient of thermal expansion of the various phases.

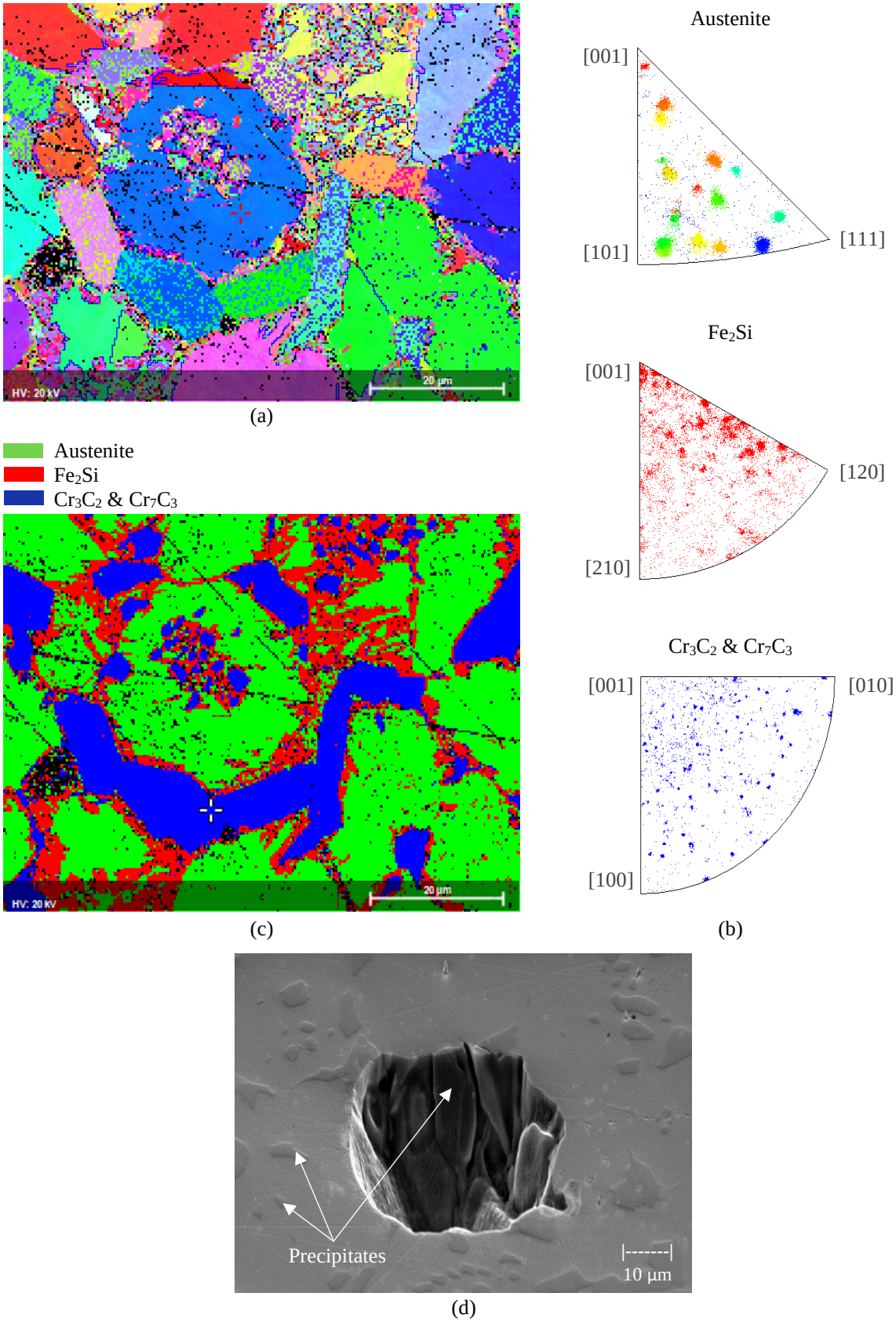

Figure 8 Microstructure of the 316L-6wt.%SiC composite. (a) EBSD inverse pole map for the normal direction and (b) its respective index maps, (c) phase map and (d) SEM micrograph of plasma etched surface showing irregular columnar precipitates.

4. Conclusions

Incorporation of nano SiC particles into 316L matrix was investigated. The powder mixing time was found to be an important influencing parameter for obtaining homogenous mixtures. Sintered samples produced from 316L+SiC+PVA powder mixes presented improved hardness. However, it is recommended for future optimisation that the hardness of the sintered samples could be further improved by increasing the compaction pressure and by optimising the heating profile of the furnace for example. The effect of the reinforcement on the tensile, corrosion and wear properties of these composites are important and will be considered in the future studies.

Both reinforced and non-reinforced powders presented similar flow properties such as cohesive levels. However, the reinforced powder provided higher levels of repeatability and a very stable rheology, and is relatively flow rate insensitive. This is considered to be due to the fact that the reinforced powder particles lost some of their satellites during the mixing process and also because of the coating of SiC which could act as a solid lubricant.

The development of the powder via the powder metallurgy route gave a good insight of the powders characteristics effects on the developed powder flow behaviour, and it allowed the study and consideration of numerous other factors affecting the powder development process. It is interesting therefore to investigate further the oxidation of the 316L powder and its effect on obtaining samples with improved sintered density and mechanical properties. The technique developed herein and the optimised results obtained are promising for its implementation for the production of nano-particle reinforced MMCs via the SLM and PM processing routes.

Acknowledgments

This publication has emanated from research supported by a research grant from Science Foundation Ireland (SFI) under Grant Number 16/RC/3872 and is co-funded under the European Regional Development Fund.

References

[1] Casati, R., Vedani, M., Casati, R., and Vedani, M., 2014, “Metal Matrix Composites Reinforced by Nano-Particles - A Review,” Metals, 4(1), pp. 65–83.
[2] Zhou, D., Qiu, F., Wang, H., Jiang, Q., Zhou, D., Qiu, F., Wang, H., and Jiang, Q., 2014, “Manufacture of Nano-Sized Particle-Reinforced Metal Matrix Composites: A Review, Manufacture of Nano-Sized Particle-Reinforced Metal Matrix Composites: A Review,” Acta Metall. Sin. Lett., 27(5), pp. 798–805.
[3] Fernandes, M. R. P., Martinelli, A. E., Klein, A. N., Hammes, G., Binder, C., and Nascimento, R. M., 2017, “Production of Nickel Matrix Composites Reinforced with Carbide Particles by Granulation of Fine Powders and Mechanical Pressing,” Powder Technol., 305, pp. 673–678.
[4] Thandalam, S. K., Ramanathan, S., and Sundarrajan, S., 2015, “Synthesis, Microstructural and Mechanical Properties of Ex Situ Zircon Particles (ZrSiO4) Reinforced Metal Matrix Composites (MMCs): A Review,” J. Mater. Res. Technol., 4(3), pp. 333–347.
[5] Munir, K. S., Kingshott, P., and Wen, C., 2015, “Carbon Nanotube Reinforced Titanium Metal Matrix Composites Prepared by Powder Metallurgy—A Review,” Crit. Rev. Solid State Mater. Sci., 40(1), pp. 38–55.
[6] Shirvanimoghaddam, K., Hamim, S. U., Karbalaei Akbari, M., Fakhrhoseini, S. M., Khayyam, H., Pakseresht, A. H., Ghasali, E., Zabet, M., Munir, K. S., Jia, S., Davim, J. P., and Naebe, M., 2017, “Carbon Fiber Reinforced Metal Matrix Composites: Fabrication Processes and Properties,” Compos. Part Appl. Sci. Manuf., 92, pp. 70–96.
[7] Nassar, A. E., and Nassar, E. E., 2017, “Properties of Aluminum Matrix Nano Composites Prepared by Powder Metallurgy Processing,” J. King Saud Univ. - Eng. Sci., 29(3), pp. 295–299.
[8] Strondl, A., Lyckfeldt, O., Brodin, H., and Ackelid, U., 2015, “Characterization and Control of Powder Properties for Additive Manufacturing,” JOM, 67(3), pp. 549–554.
[9] Azevedo, J. M. C., CabreraSerrenho, A., and Allwood, J. M., 2018, “Energy and Material Efficiency of Steel Powder Metallurgy,” Powder Technol., 328, pp. 329–336.
[10] Riou, A., Aumund, C., and Erasteel, O., 2015, “Introduction to Additive Manufacturing Technology: A Guide for Designers and Engineers,” Eur. Powder Metall. Assoc., 1st Edition, pp. 01–44.
[11] Clyne, T. W., 2001, “Composites: Interfaces,” *Encyclopedia of Materials: Science and Technology*, K.H.J. Buschow, R.W. Cahn, M.C. Flemings, B. Ilschner, E.J. Kramer, S. Mahajan, and P. Veyssière, eds., Elsevier, Oxford, pp. 1382–1391.
[12] Vani, V. V., and Chak, S. K., 2018, “The Effect of Process Parameters in Aluminum Metal Matrix Composites with Powder Metallurgy,” Manuf. Rev., 5, p. 7.

[13] Huang, L. J., Geng, L., Xu, H. Y., and Peng, H. X., 2011, "In Situ TiC Particles Reinforced Ti6Al4V Matrix Composite with a Network Reinforcement Architecture," Mater. Sci. Eng. A, 528(6), pp. 2859–2862.
[14] Huang, L. J., Geng, L., and Peng, H.-X., 2015, "Microstructurally Inhomogeneous Composites: Is a Homogeneous Reinforcement Distribution Optimal?," Prog. Mater. Sci., 71, pp. 93–168.
[15] Shahid, R. N., and Scudino, S., 2018, "Strengthening of Al-Fe 3 Al Composites by the Generation of Harmonic Structures," Sci. Rep., 8(1).
[16] Bai, M., Song, B., Reddy, L., and Hussain, T., 2019, "Preparation of MCrAlY–Al2O3 Composite Coatings with Enhanced Oxidation Resistance through a Novel Powder Manufacturing Process," J. Therm. Spray Technol., 28(3), pp. 433–443.
[17] Song, B., Wang, Z., Yan, Q., Zhang, Y., Zhang, J., Cai, C., Wei, Q., and Shi, Y., 2017, "Integral Method of Preparation and Fabrication of Metal Matrix Composite: Selective Laser Melting of in-Situ Nano/Submicro-Sized Carbides Reinforced Iron Matrix Composites," Mater. Sci. Eng. A, 707, pp. 478–487.
[18] Gu, D., Wang, H., and Zhang, G., 2014, "Selective Laser Melting Additive Manufacturing of Ti-Based Nanocomposites: The Role of Nanopowder," Metall. Mater. Trans. A, 45(1), pp. 464–476.
[19] Zhang, F., Mei, M., Al-Hamdani, K., Tan, H., and Clare, A. T., 2018, "Novel Nucleation Mechanisms through Satelliting in Direct Metal Deposition of Ti-15Mo," Mater. Lett., 213, pp. 197–200.
[20] Martin, J. H., Yahata, B. D., Clough, E. C., Mayer, J. A., Hundley, J. M., and Schaedler, T. A., 2018, "Additive Manufacturing of Metal Matrix Composites via Nanofunctionalization," MRS Commun., 8(2), pp. 297–302.
[21] Black, J. T., and kohser, R. A., 2011, *Materials and Processes in Manufacturing*, John Wiley & Sons, United States of America.
[22] Asthana, R., Kumar, A., and Dahotre, N. B., 2006, *Materials Processing and Manufacturing Science*, Elsevier, United States of America.
[23] Spierings, A. B., Voegtlin, M., Bauer, T., and Wegener, K., 2016, "Powder Flowability Characterisation Methodology for Powder-Bed-Based Metal Additive Manufacturing," Prog. Addit. Manuf., 1(1), pp. 9–20.
[24] Baitimerov, R., Lykov, P., Zherebtsov, D., Radionova, L., Shultc, A., and Prashanth, K. G., 2018, "Influence of Powder Characteristics on Processability of AlSi12 Alloy Fabricated by Selective Laser Melting," Materials, 11(5).
[25] Freeman, R., 2007, "Measuring the Flow Properties of Consolidated, Conditioned and Aerated Powders - A Comparative Study Using a Powder Rheometer and a Rotational Shear Cell," Powder Technol., 174(1), pp. 25–33.
[26] Krantz, M., Zhang, H., and Zhu, J., 2009, "Characterization of Powder Flow: Static and Dynamic Testing," Powder Technol., 194(3), pp. 239–245.
[27] Liu, B., Wildman, R., Tuck, C. R., Ashcroft, I., and Hague, R. J. M., 2011, "Investigation the Effect of Particle Size Distribution on Processing Parameters Optimisation in Selective Laser Melting Process," Additive Manufacturing Research Group, Loughborough University.
[28] Hatami, S., Lyckfeldt, O., Tönnäng, L., and Fransson, K., 2017, "Flow Properties of Tool Steel Powders for Selective Laser Melting – Influence of Thermal and Mechanical Powder Treatments," Powder Metall., 60(5), pp. 353–362.
[29] Clayton, J., 2014, "Optimising Metal Powders for Additive Manufacturing," Met. Powder Rep., 69(5), pp. 14–17.
[30] Nguyen, Q. B., Nai, M. L. S., Zhu, Z., Sun, C.-N., Wei, J., and Zhou, W., 2017, "Characteristics of Inconel Powders for Powder-Bed Additive Manufacturing," Engineering, 3(5), pp. 695–700.
[31] Ludwig, B., and Miller, T. F., 2015, "Rheological and Surface Chemical Characterization of Alkoxysilane Treated, Fine Aluminum Powders Showing Enhanced Flowability and Fluidization Behavior for Delivery Applications," Powder Technol., 283, pp. 380–388.
[32] Sotomayor, M. E., Várez, A., and Levenfeld, B., 2010, "Influence of Powder Particle Size Distribution on Rheological Properties of 316L Powder Injection Moulding Feedstocks," Powder Technol., 200(1), pp. 30–36.
[33] Pleass, C., and Jothi, S., 2018, "Influence of Powder Characteristics and Additive Manufacturing Process Parameters on the Microstructure and Mechanical Behaviour of Inconel 625 Fabricated by Selective Laser Melting," Addit. Manuf., 24, pp. 419–431.
[34] Yun, H., Dong, L., Wang, W., Bing, Z., and Xiangyun, L., 2018, "Study on the Flowability of TC4 Alloy Powder for 3D Printing," Mater. Sci. Eng., 439.
[35] Tan, J. H., Wong, W. L. E., and Dalgarno, K. W., 2017, "An Overview of Powder Granulometry on Feedstock and Part Performance in the Selective Laser Melting Process," Addit. Manuf., 18, pp. 228–255.
[36] Liu, J., Silveira, J., Groarke, R., Parab, S., Singh, H., McCarthy, E., Karazi, S., Mussatto, A., Houghtaling, J., Ahad, I. U., Naher, S., and Brabazon, D., 2019, "Effect of Powder Metallurgy Synthesis Parameters for Pure Aluminium on Resultant Mechanical Properties," Int. J. Mater. Form., 12(1), pp. 79–87.

[37] Gülsoy, H. Ö., 2008, "Production of Injection Moulded 316L Stainless Steels Reinforced with TiC(N) Particles," Mater. Sci. Technol., 24(12), pp. 1484–1491.
[38] Gülsoy, H. Ö., Baykara, T., and Özbek, S., 2011, "Injection Moulding of 316L Stainless Steels Reinforced with Nanosize Alumina Particles," Powder Metall., 54(3), pp. 360–365.
[39] Klar, E., and Samal, P. K., 2007, *Powder Metallurgy Stainless Steels: Processing, Microstructures, and Properties*, ASM International, Ohio.
[40] Larsen, R. M., and Thorsen, K. A., 1994, "Equilibria and Kinetics of Gas–Metal Reactions During Sintering of Austenitic Stainless Steel," Powder Metall., 37(1), pp. 61–66.
[41] Arh, B., and Tehovnik, F., 2007, "The Oxidation and Reduction of Chromium during the Elaboration of Stainless Steels in an Electric Arc Furnace," Mater. Technol., 41(5), pp. 203–211.
[42] Buffat, P. A., and Borel, J. P., 1976, "Size Effect on the Melting Temperature of Gold Particles," Phys. Rev. A, 13(6), pp. 2287–2298.
[43] Lai, S. L., Guo, J. Y., Petrova, V., Ramanath, G., and Allen, L. H., 1996, "Size-Dependent Melting Properties of Small Tin Particles: Nanocalorimetric Measurements," Phys. Rev. Lett., 77(1), pp. 99–102.
[44] Little, S. A., Begou, T., Collins, R. W., and Marsillac, S., 2012, "Optical Detection of Melting Point Depression for Silver Nanoparticles via in Situ Real Time Spectroscopic Ellipsometry," Appl. Phys. Lett., 100(5).
[45] Sun, J., and Simon, S. L., 2007, "The Melting Behavior of Aluminum Nanoparticles," Thermochim. Acta, 463(1), pp. 32–40.
[46] Meyyappan, M., and Sunkara, M. K., 2009, *Inorganic Nanowires: Applications, Properties, and Characterization*, CRC Press, London.
[47] Yang, C., Wong, C. P., and Yuen, M. M. F., 2013, "Printed Electrically Conductive Composites: Conductive Filler Designs and Surface Engineering," J. Mater. Chem. C, 1(26), pp. 4052–4069.
[48] Allen, G. L., Bayles, R. A., Gile, W. W., and Jesser, W. A., 1986, "Small Particle Melting of Pure Metals," Thin Solid Films, 144(2), pp. 297–308.
[49] Menamparambath, M. M., Muhammed Ajmal, C., Kim, K. H., Yang, D., Roh, J., Park, H. C., Kwak, C., Choi, J.-Y., and Baik, S., 2015, "Silver Nanowires Decorated with Silver Nanoparticles for Low-Haze Flexible Transparent Conductive Films," Sci. Rep., 5.
[50] El Fawkhry, M. K., and Mattar, T., 2018, "Influence of Diffusion and Wetting on the SiC Reinforcement of the Cast Surface of Low Alloy Steel," Int. J. Met., 12(1), pp. 139–147.
[51] Wu, C. L., Zhang, S., Zhang, C. H., Zhang, J. B., Liu, Y., and Chen, J., 2019, "Effects of SiC Content on Phase Evolution and Corrosion Behavior of SiC-Reinforced 316L Stainless Steel Matrix Composites by Laser Melting Deposition," Opt. Laser Technol., 115, pp. 134–139.
[52] Carvalho, O., Madeira, S., Buciumeanu, M., Soares, D., Silva, F., and Miranda, G., 2016, "Pressure and Sintering Temperature Influence on the Interface Reaction of SiCp/410L Stainless Steel Composites," J. Compos. Mater., 50(15), pp. 2005–2015.
[53] Sorbello, F., Flewitt, P. E. J., Crocker, A. G., and Smith, G. E., 2008, "A Consideration of Cleavage Crack Propagation in Fe2Si Steel," Key Eng. Mater.
[54] Mari, D., Miguel, L., and Nebel, C., 2014, *Comprehensive Hard Materials*, Newnes.
[55] Chattopadhyay, R., 2001, *Surface Wear: Analysis, Treatment, and Prevention*, ASM International.
[56] Buytoz, S., 2006, "Microstructural Properties of SiC Based Hardfacing on Low Alloy Steel," Surf. Coat. Technol., 200(12), pp. 3734–3742.